RSC Advances

ROYAL SOCIETY OF CHEMISTRY

www.rsc.org/advances

Battling Absorptive Losses by Plasmon-Exciton Coupling in Multimeric Nanostructures

Alireza Rahimi Rashed[a,b,*], *Antonio De Luca*[b], *Rakesh Dhama*[b], *Arash Hosseinzadeh*[c], *Melissa Infusino*[a,d], *Mohamed El Kabbash*[a], *Serge Ravaine*[e], *Roberto Bartolino*[b,f] *and Giuseppe Strangi*[a,b,*]

[a]Department of Physics, Case Western Reserve University, 2076, Adelbert Road, Cleveland Ohio, 44106-7079, USA

[b]Department of Physics, University of Calabria, IPCF-CNR UOS di Cosenza, Licryl Laboratory, 87036 - Rende (CS), Italy

[c]Department of Electrical and Computer Engineering, Michigan Technological University, Houghton, MI 49931, USA

[d]Colegio de Ciencias e Ingeniería, Universidad San Francisco de Quito, Avenida Vía Lactea,Quito, Ecuador

[e]Centre de Recherche Paul Pascal (CNRS-UPR8641), 115 av. Dr A. Schweitzer, 33600 Pessac, France

[f]Centro Linceo Interdisciplinare B. Segre, Accademia Nazionale dei Lincei Rome, Palazzo Corsini - Via della Lungara, 10 – 00165, Roma, Italy

* Address correspondence to:

(G. Strangi) giuseppe.strangi@case.edu

(A. Rahimi Rashed) alireza.rahimirashed@case.edu

Abstract: The inherent and strong optical losses present in plasmonic nanostructures, significantly limits their technological applications at optical frequencies. Here, we report about the interplay between plasmons and excitons as a potential approach to selectively reduce ohmic losses. Samples have been prepared by functionalizing plasmonic core-shell nanostructures with excitonic molecules embedded in silica shells and interlocked by silica spacers to investigate the role played by the plasmon-exciton elements separation. Results obtained for different silica spacer thicknesses are evaluated by comparing dispersions of plasmonic multimers with respect to corresponding monomers. We have measured fluorophores emission quenching by means of steady-state fluorescence spectroscopy and as well as significant shortening of the corresponding fluorescence lifetime. These results were accompanied by simultaneous enhancement of Rayleigh scattering and transmittance, revealing an effective absorptive loss mitigation of the multimeric systems. Moreover, upon decreasing the thickness of the intermediate silica layer between gold cores and the external gain functionalized silica shell, the efficiency of exciton-plasmon resonant energy transfer (EPRET) was significantly enhanced in both multimeric and monomeric samples. Simulations data along with experimental results confirm that the hybridized plasmon fields of multimers lead to more efficient optical loss compensation with respect to corresponding monomers.

1 Introduction

In the past decade, plasmonic nanostructures have attracted great interest because of their extraordinary and promising physical properties, assuming an important role in emerging science and technological applications. In particular, the wide cross-disciplinary features of the plasmonics are emerging in new research fields leading to interesting fundamental aspects and promising applications in materials science, biology and medicine.

It is well known that the particular optical properties of noble metal nanoparticles (NPs) are attributed to the localized surface plasmon resonance (LSPR), which is the collective coherent oscillation of free electrons (with respect to the positive ionic background) on the metal surface in resonance with the electric component of an incident electromagnetic wave. LSPR contributes to strong confinement of optical radiation and large enhancement of the electromagnetic field in their proximity. Current research efforts in nanoplasmonics led to various photonics, opto-electronic and biomedical applications such as single-particle detection and biomolecular recognition,[1,2] optical probes for high resolution imaging,[3] photo-thermal therapies,[4] photovoltaics,[5] Raman biosensing,[6-8] colorimetric sensing,[9] hyper-lenses,[10] and optical metamaterials.[11-13] Negative values of the real part and low values of the imaginary part of the dielectric permittivity are key for plasmonic applications. However, plasmonic NPs are not ideal resonators and exhibit considerable ohmic losses at optical wavelengths that are undesired for most of the potential applications.

In this respect, some theoretical[13-16] and experimental studies[17-19] have demonstrated how non-radiative resonant energy transfer (RET) processes may play a role in modifying the imaginary part of the effective dielectric function of the hybrid systems. Non-radiative energy transfer efficiency in hybrid systems (plasmon-exciton) strongly depends on physical

parameters[20-26] such as: (i) the geometry and size of the metal nanostructures, (ii) inter-particle distance, (iii) relative spectral position between excitonic band and surface plasmon band (SPB) of metal NPs, (iv) relative orientation of chromophores transition dipole moment with respect to NPs plasmon mode, (v) strength of transition dipole moment, (vi) concentration and concentration and molar extinction coefficient of the plasmonic and excitonic particles. Recently, Bo Peng *et al.*[18] have reported that the incorporation of gain material at a controlled distance from gold NPs, allows to control and optimize RET mechanisms. In our former studies, we have investigated the influence of incorporation of excitonic material (chromophores) in the high-local-field areas of plasmon nanostructures to induce coherent RET processes from chromophores (donors) to plasmon nano-entities (acceptors), both in gain assisted (NP-dye dispersions) and gain-functionalized (dye encapsulated into the silica shell) systems.[27-29]

In the present study, we have investigated NP dispersions of multimeric (e.g., monomers, dimers, trimers, quadrimers, etc.) nanostructures consisting of gold-core/silica spacer/silica shell, in which chromophores (Rhodamine B by Exciton) have been grafted at the interface between silica spacer and the protective external shell. By varying the intermediate silica shell thickness from 10 to 30 nm, two series of multimeric nanostructures have been synthesized and dissolved in ethanol solution: passive (without chromophores) and active (functionalized with chromophores). In addition, corresponding passive and active single NPs (monomers) have been synthesized and used as control samples.

Steady-state fluorescence spectroscopy accompanied by ultrafast time resolved spectroscopy show a stronger coherent coupling between plasmonic cores and embedded excitonic molecules in multimers as compared to the similar monomers. Moreover, Rayleigh scattering measurements and transient absorption spectroscopy, performed on these two sets of

samples, show a stronger plasmon-exciton coupling in multimeric nanostructures with respect to single nanoparticles (monomers), revealing a stronger optical loss mitigation in the case of multimeric nanostructures. Simulation results demonstrate the occurrence of an enhanced local field in multimers with respect to equivalent monomers which can be understood within the context of plasmon hybridization theory in multimeric nanostructures.[30-34] However, we found that shorter separation distance between NP and dye molecules may lead to more efficient non-radiative RET processes, which results in further absorptive losses mitigation. In addition, these results confirm that the exciton-plasmon RET processes may occur at separation distances longer than those occurring for[35-37] Förster resonant energy transfer (FRET).[38]

2 Results and Discussion

In this experimental study, two categories of multi-silica shell NPs have been investigated: Active and passive multimeric and monomeric nanostructures (control samples). Passive NPs consist of ethanol solutions of gold-core 60 nm in diameter, coated with silica shells 10 and 30 nm thick, labeled as Mo10 and Mo30, respectively. Correspondingly active NPs, namely Mo+10 and Mo+30, have been synthesized by starting from Mo10 and Mo30 samples, then grafting via click chemistry Rhodamine B isothiocyanate (RhB) dye molecules onto the spacer silica shell. Finally, a second 10 nm protective silica shell is used to cover all samples and protect the RhB molecules on Mo+10 and Mo+30 samples.

At the same time, multimeric samples have been produced by selecting monomers, dimers, trimers, quadrimers, heptamers, etc, of both passive and active monomers with 10 and 30 nm plasmon-chromophore separation distances. Active multimers (main samples) and

corresponding passive ones (control samples) have been labeled as Mu+10, Mu+30 and Mu10, Mu30, respectively. A sketch of multimeric system is presented in Fig. 1a.

Monodispersity of monomeric samples and uniformity in size and shape of both systems have been investigated by means of transmission electron microscopy (TEM) (TEM) technique (Fig. 1c and 1d). Average size uniformity is obtained by statistical analysis of the core diameter, as shown in Fig. 1b. Further information regarding the core size and silica shell thickness is provided in the Methods section.

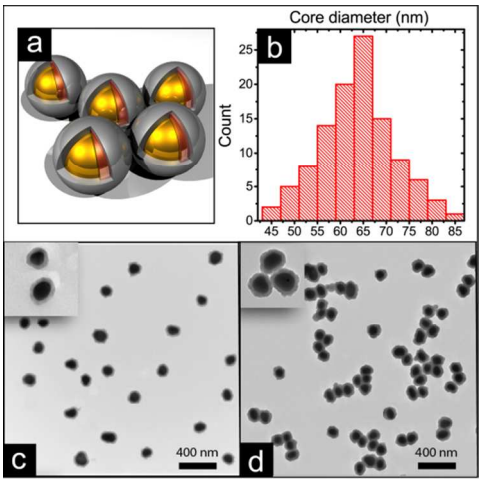

Fig. 1 a) Sketch of the active multimers **b)** statistical analysis of core diameters performed on Mu+10 system. TEM images of the **c)** Mo+10 monomers and **d)** Mu+10 multimers with core diameter of 60 nm, silica spacer of 10 nm and silica protective shell of 10 nm.

The extinction cross-section spectra of both systems have been measured. Fig. 2(a) and 2b show the normalized extinction cross-section profiles of both passive and active monomers and multimers, respectively. It is well known that the plasmon response of the nanostructures can be influenced by the thickness of the silica shell, refractive index of the surrounding environment and configuration of nanostructures.[39,40] In Fig. 2(a) and 2(b), the SPBs show a slight red-shift for multimeric systems with respect to monomeric ones. The increase of the local field intensity due to coherent plasmon-plasmon interactions leading to hybridization processes[30-32] can result

in a more efficient scattering cross-section of multimers accompanied by a significant red-shift with respect to the absorption efficiency spectrum.[41] Of note is the increase of the red-shift of the extinction curves for multimers with respect to monomers, for shorter gold core-fluorophores separation (10 nm) as compared to thicker separation layer samples.

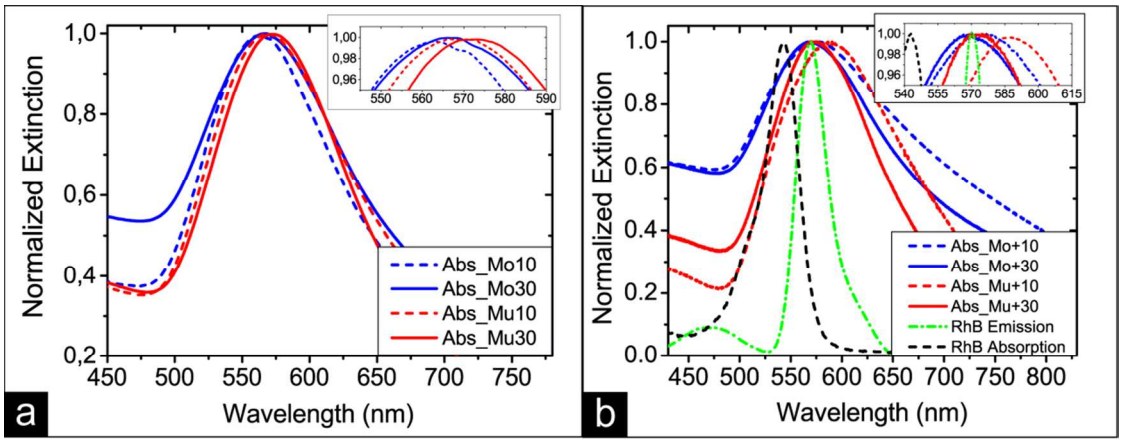

Fig. 2 Normalized Extinction spectra of **a)** passive and **b)** active monomers and multimers, including absorption ($\lambda_{abs,max}$ = 543 nm) and emission ($\lambda_{em,max}$ = 570 nm) spectra of RhB dye molecules all dispersed in ethanol. Insets of Fig. 2(a) and 2(b) precisely show the red-shift of multimers plasmon band as compared to that of corresponding monomers.

2.1 Numerical Calculation Results

In order to qualitatively investigate the effect of the local field enhancement on the plasmon-exciton coupling efficiency the local field distribution of both active monomers and multimers are simulated by full wave electromagnetic simulation software based on finite element method (FEM) (see Methods for details). The electromagnetic properties of the gain material have been modeled by a generic four-level system described by a standard semi-classical equivalent model.[42-43] This approach allows us to simulate the plasmon-exciton coupling in the same experimental conditions in which the dye molecules are excited. The approximate active constitutive relation for a gain medium in the linear regime is expressed by the following Lorentzian dispersion formula[44]

$$\varepsilon_g \sim \varepsilon_0\varepsilon_h + \frac{\sigma_a}{\omega^2 + i\omega\Delta\omega_a - \omega_a^2}\frac{\tau_{21}\Gamma_{pump03}}{1+\tau_{21}\Gamma_{pump03}}N_0 \ , \quad (1)$$

$\Delta\omega_a$ is the bandwidth of the dye transition at the emitting angular frequency ω_a, σ_a is the coupling strength of polarization density of gain to the external electric field, τ_{21} is the decay rate of fluorophores from the metastable energy level, Γ_{pump03} is the pumping rate from level 0 to level 3 and ε_h stands for the permittivity of the environment, surrounding gain elements.

Simulations of normalized local field intensity (ψ) of both plasmonic systems are showed in Fig. 4, in which $\psi = |E/E_i|^2$ is the absolute ratio of the local field intensity (E^2) surrounding a nanostructure calculated at maximum fluorophore emission intensity wavelength, with respect to the intensity of incident plane wave field (E_i^2). The obtained results demonstrate that gain functionalized plasmonic systems generate the amplification of local fields with respect to passive ones, as evident upon comparing ψ values for active monomers in Fig. 3(c) and 3(d) with equivalent passive nanostructures in Fig. 3(a) and 3(b). Such enhancement is due to the near field coupling between the dipoles of plasmons and excitons, resulting from satisfying the aforementioned PRET conditions.

In addition, the retrieved local field intensity of gain functionalized samples having different thicknesses of the silica spacer: 10 nm (Fig. 3(c), 3(e), 3(g), 3(i) and 3(k)) and 30 nm (Fig. 3(d), 3(f), 3(h), 3(j) and 3(l)) silica spacers. In fact, plasmonic local field of thinner silica spacer nanostructures (10 nm) is much more intense, providing better conditions for plasmon-exciton coupling. Moreover, these numerical calculations predict that the multimeric configurations are promising plexcitonic systems for enhanced near fields as a consequence of the plasmon hybridization effect. Plasmon hybridized modes originate from linear interaction of the fundamental plasmon modes of the individual NPs, in analogy to molecular orbital

theory.[45,46] Such combination leads to the splitting of the plasmon resonances into two new resonances, the lower energy symmetric or "bonding" plasmon and the higher energy anti-symmetric or "anti-bonding" plasmon.[31,32,46] As the gap between NPs decreases the coherent (bonding) mode is more pronounced with respect to the anti-bonding one, as a result of the increasing energy difference between two modes. The presence of such a strong coherent mode results in a stronger field intensity in multimeric systems.

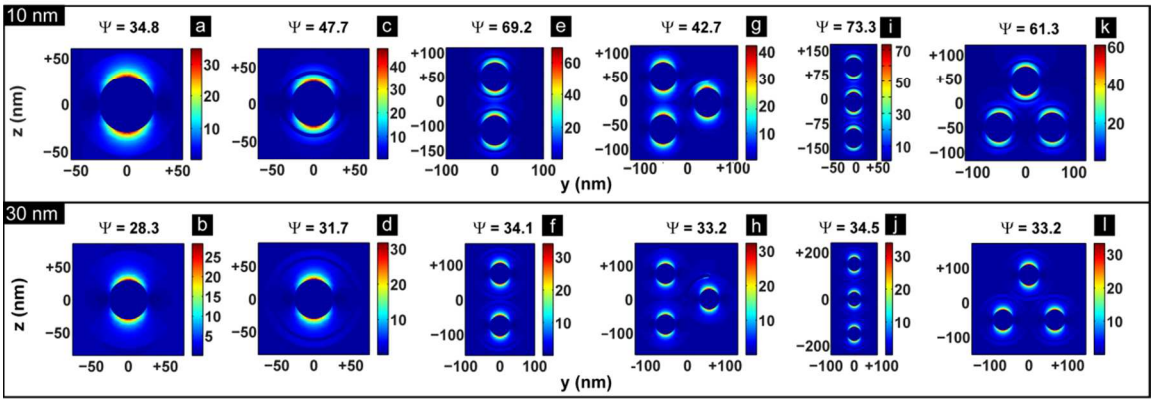

Fig. 3 Simulation results for local field intensity of **a)** passive monomers; Active **c)** monomers, **e)** dimers, **g)** trimers (orientation 1), **i)** aligned trimers **k)** trimers (orientation 2) with 10 nm silica shell thickness, and **b)** passive monomers; Active **d)** monomers, **f)** dimers, **h)** trimers (orientation 1), **j)** aligned trimers, **l)** trimers (orientation 2) with 30 nm silica shell thickness. The normalized field profiles (ψ) are calculated at the maximum emission wavelength of RhB dye molecules in ethanol and plotted in YZ cross section plane (for detail see Methods section).

2.2 Experimental Results

Steady-state fluorescence measurements have been performed on the investigated systems. As evidenced from Fig. 4, the emission spectral position of encapsulated RhB in our NPs shows a significant change with respect to the same molecules dispersed in solution (green dashed dotted line in Fig. 2b). In fact, the surrounding environment[47] and probable formation of dye aggregates during grafting process can modify the absorption and emission curves.[48]

Moreover, excited dye molecules exposed to intense plasmonic fields may undergo radiative decay from energy levels triggered by plasmon modes. Steady-state photoluminescence

(PL) studies show that the fluorescence peak corresponding to multimers is red-shifted with respect to the monomers (Fig. 4a and b), This effect appears more pronounced in Mu+10 sample (thinner silica spacer thickness) as compared to Mu+30, corroborating our hypothesis that strong plasmon fields can trigger radiative resonant with the plasmon modes, that are expected to be at longer wavelength for Mu+10 (see Fig. 2b).

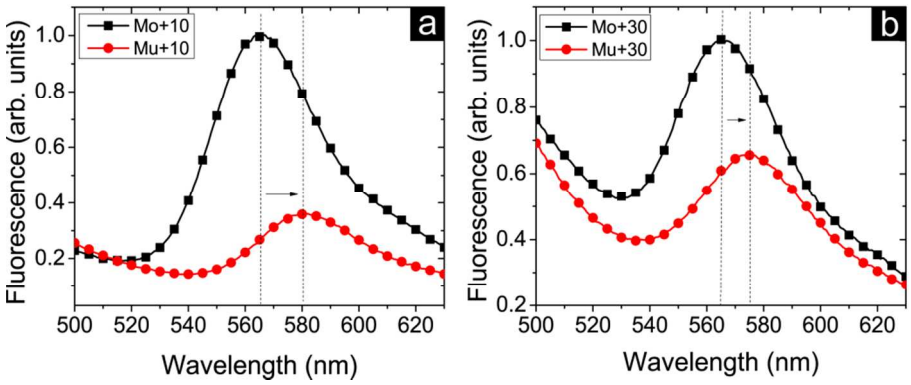

Fig. 4 Fluorescence quenching observed in multimers as compared to monomers under the same pump energy value. **a)** Fluorescence emission maxima of Mo+10 sample (black squares) with respect to Mu+10 sample (red circles). **b)** Fluorescence emission maxima of the Mo+30 sample (black squares) with respect to Mu+30 sample (red circles).

In addition, fluorescence quenching effects can be observed because of resonant non-radiative energy transfer processes between excited fluorophores and plasmon nanostructures. We have observed fluorescence quenching of RhB dye molecules in both multimeric systems. Emission spectra of gain materials grafted in Mu+10 sample show a 2.8 fold intensity reduction compared with Mo+10 (Fig. 4a), whereas only 1.5 fold lowering was observed in Mu+30 (Fig. 4b). The obtained results demonstrate that fluorescence quenching process is more efficient in multimers with thinner spacer, because of the more effective EPRET process in the case that excitonic molecules are placed in close proximity to plasmon NPs.

To perform a systematic study of gain-induced optical loss modifications, time-resolved fluorescence spectroscopy,[49-51] transmission and Rayleigh scattering spectroscopies have been performed on both monomeric and multimeric systems.

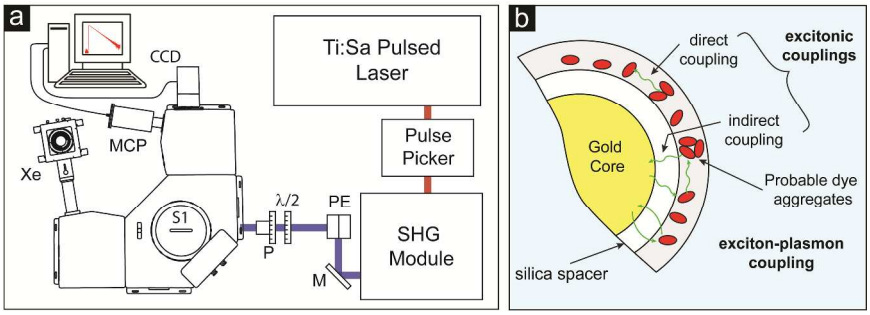

Fig. 5 a) Scheme of the spectrofluorometer set up to perform ultrafast time-resolved fluorescence spectroscopy. **b)** Sketch of different coupling configurations between grafted dye molecules and gold cores.

Fluorescence lifetime of all samples has been measured and compared with pure dye solution. In Fig. 5(a) is shown the scheme of the ultrafast time resolved spectroscopy[50] setup used to acquire time-correlated single-photon counting (TCSPC) data from active samples (see Methods for details of the setup). The fluorescence time decay of dissolved RhB molecules was fitted by a single exponential function, while for both monomeric and multimeric systems the time decay curves were fitted by using tri-exponential decay functions (green dots and blue line fit in Fig. 6). The fitting procedure of the emission intensity decays $I(t)$, uses a tri-exponential model according to the following expression:

$$I(t) = \sum_{i=1}^{3} \alpha_i exp(-t / \tau_i) \ , \qquad (2)$$

Where τ_i are the decay times and α_i represent the amplitudes of each component at t = 0.[47] The presence of a very fast decay time (τ_1) is attributed to a significant enhancement of the non-radiative decay rate due to a strong EPRET processes as represented in Fig. 5(b). The intermediate decay time (τ_2) is related to FRET interactions, which may occur via two main coupling channels: direct coupling (*i.e* the excitonic coupling) and indirect coupling (*i.e* the excitonic coupling assisted by the plasmon).[52-54] Finally, the long-living emission decay kinetics (τ_3) are attributed to a small percentage of unbound dye molecules that may have persisted

throughout purification of samples or those dye molecules which have not participated in energy transfer processes.

For an ethanolic solution of RhB molecules, time-resolved fluorescence decay curve (black line in Fig. 6(a) and 6(b)) can be fitted with a single-exponential function resulting in a lifetime of about $\tau_D \sim 3$ ns ($\chi^2 = 1.192$). The observed results are consistent with previous studies which have been performed in RhB doped silica beads.[55]

Fig. 6 compares the TCSPC data obtained at 572 nm, for dye molecules functionalized in monomeric (green lines) and multimeric (red lines) systems when irradiated with 375 nm ultrafast pulsed laser. The results of TCSPC data fit of these samples (Fig. 6, blue dots for monomers and black dots for multimers) are presented in Table 1.

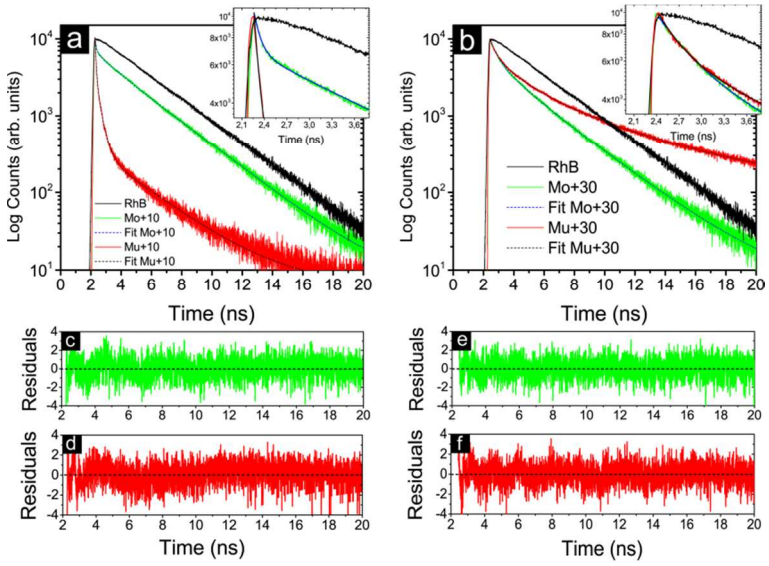

Fig. 6 Time-resolved fluorescence decays and relative fitting plots of **a)** monomer (Mo+10) and multimer (Mu+10) systems. **b)** Monomer (Mo+30) and multimer (Mu+30) systems. **c-f)** Show residuals decay fit of Mo+10 and Mu+10 systems and of Mo+30 and Mu+30 systems, respectively.

The experimental data show a significant reduction of the living time of exciton states in multimeric systems with respect to a single NP (monomer), reflecting a stronger plexcitonic coupling in multimers. The obtained results are in agreement with the steady-state fluorescence

spectroscopy data, where multimers show a higher fluorescence quenching efficiency with respect to the corresponding monomers (Fig. 4), and also corroborated by numerical simulations of local field intensities presented in Fig. 3, as the plasmon-exciton coupling strength is mediated by the enhanced local field of multimers. Besides the direct coupling between fluorophores embedded in a single NP, the nanospheres constituting a multimeric structure enhance the indirect coupling between dye molecules via the plasmonic gold core, which results in a shortening of τ_2 for the case of Mu+10 as compared to Mo+10. The long-living emission decay times τ_3 of both samples are almost the same, being associated to the fluorescence decay time of non-interacting supernatant dye molecules.

Sample	λ_{ex} (nm)	λ_{em} (nm)	τ_1 (ps)	τ_2 (ps)	τ_3 (ns)	χ^2
Mu+10	375	572	70 ± 1	332 ± 3	3.00 ± 0.01	1.27
Mo+10	375	572	88 ± 2	971 ± 56	2.90 ± 0.01	1.14
Mu+30	375	572	325 ± 7	1582 ± 40	5.32 ± 0.01	1.18
Mo+30	375	572	452 ± 10	1860 ± 20	3.2 ± 0.1	1.07

Table 1 Time resolved fluorescence decay results for monomeric and multimeric systems with 10 nm and 30 nm fluorophores-NP separation distances. λ_{ex} and λ_{em} stand for excitation and emission wavelengths, respectively. τ_1, τ_2 and τ_3 are the components of the tre-exponential function used to fit the TCSPC data correlated to each one of active sample. χ^2 is the chi-square function which shows the goodness of the applied fit.

A comparative set of lifetime measurements has been performed even on Mo+30 and Mu+30 nanostructures, where chromophores are located 30 nm apart from gold cores (see Table 1). The acquired lifetime of Mo+30 and Mu+30 systems reveal that Mu+30 samples show a reduction in both short- and intermediate-living times with respect to Mo+30 monomers, indicating the occurrence of a more effective dye-NP and dye-dye couplings in Mu+30 system.

Hence, these data indicate that: i) non-radiative RET processes occur between chromophores and metal cores leading to very short living times (τ_1); ii) plasmon-exciton RET is drastically affected by their separation distance; iii) as a result of plasmon hybridization process, multimeric systems generally create more intense plasmonic hot-spots (high local fields), providing stronger plasmon-exciton coupling with respect to monomeric systems. iv) the intermediate decay times (τ_2) infer that the decrease of silica shell thickness, as well as enhanced local fields further promotes indirect couplings, irrespective of monomeric or multimeric systems; v) these results show that energy transfer processes between exciton and plasmon states, occur over 30 nm of separation distances. The presence of RET for such inter-distances proves that in contrast to FRET (max inter-distance 10 nm), plexcitonic RET can occur even for longer interparticle distances, up to 30 - 40 nm.

In order to gain further understandings concerning the effects related to the interplay between excitons and plasmons in the investigated systems, pump–probe experiments have been performed. According to the Beer–Lambert law, by measuring simultaneously Rayleigh scattering and transient absorption, both in the absence and in presence of gain, allow us to determine if the extinction curve of the plasmonic structure is affected by resonant energy transfer processes.

Thus, modifications of Rayleigh scattering and transmitted intensity of probe beams have been monitored as a function of the pump energy for all systems (excitation wavelength = 355 nm). A pin-hole and a notch filter were used just before spectrometer; in order to avoid that stray light may affect the experiment. The pumping wavelength was selected to avoid direct excitation of the NP plasmon states and to excite only the RhB dye molecules. We have also made sure that

the optical pumping was not inducing significant changes in the sample by measuring transmitted and scattering intensity before and after pumping events.

As first proposed by Lawandy,[56] the localized SP resonance in metallic nanospheres is expected to show a singularity when the surrounding dielectric medium provide a critical value of optical gain. This can be evidenced by an increase in the Rayleigh scattering signal because of the enhancement of the local field around the metal nano-antenna. Pump–probe Rayleigh scattering experiments have been performed by launching collinearly a probe beam in a small portion of the volume excited by a pump beam at $\lambda = 355$ nm. The modification of the scattered probe beam is detected at an angle of 70° relative to the beam propagation direction. The scattered probe light, acquired by means of the optical fiber of a high-resolution spectrometer (HORIBA Jobin-Yvon MicroHR Symphony), was observed in the spectrum as a relatively narrow line centered at 532 nm.

Fig. 7(a) shows the enhancement of Rayleigh scattering signal as a function of excitation energy in Mu+10 multimers. The increase of the scattered signal above a given threshold value of the pump energy demonstrates the enhancement of the Rayleigh scattering cross section mediated by EPRET processes.[27-29] Finally, we have measured the transmittance of the probe beam traversing the excited volume upon varying the pump rate and comparing with the transmittance in the absence of excitation. Fig. 7(b) shows the increase of transmission peaks of the probe signal at 532 nm as a function of the excitation energy for Mu+10 system. Accordingly, as mentioned earlier, the simultaneous enhancement of Rayleigh scattering and optical transmittance imply the mitigation of absorptive losses, specifically in Mu+10 hybrid system.

Fig. 7(c) and 7(d) show the enhancement of the Rayleigh scattering intensity and optical transmission at 532 nm, as a function of the pump rate, for Mu+30 sample. Such a phenomenon confirms the inter-distance dependence of the non-radiative energy transfer rate among NP-chromophore according to EPRET theory, dipolar interactions are expected to scale as r^{-4}, being r the NP-chromophore separation distance.[57,58] Furthermore, critical behavior of the transmission was observed above a given threshold value of about 0.45 mJ/pulse for Mu+10, whereas the threshold value for Mu+30 was found to be about 0.63 mJ/pulse, showing a change in the RET efficiency as function of the gain.[56]

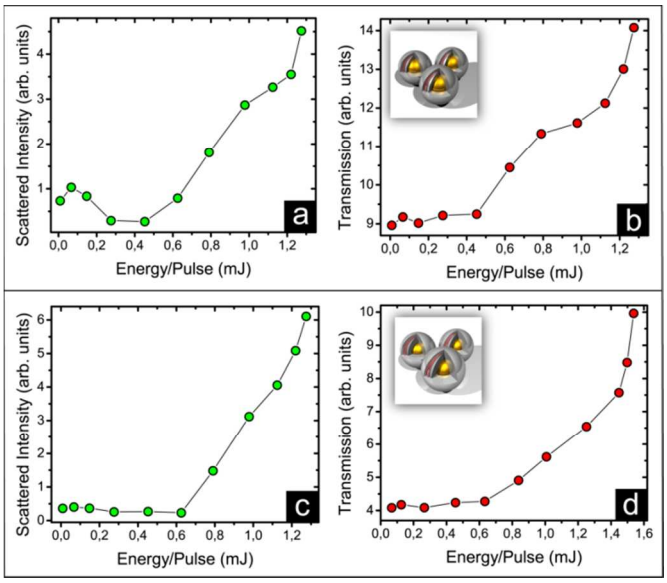

Fig. 7 Normalized Rayleigh scattering **(a,c)** and transmission **(b,d)** signals of the probe beam (532 nm) as a function of the pump energy (355 nm) for multimeric systems: **(a,b)** Mu+10 and **(c,d)** Mu+30. Lower threshold values of transmittance and scattering are observed for Mu+10 system compared to Mu+30.

A comparative set of experiments, including both Rayleigh scattering and optical transmission have been performed on Mo+10 and Mo+30 monomers. The results reported in Fig. 8 indicate a striking enhancement in the scattered and transmitted light above a certain gain threshold value. Evidently, Mo+10 system demonstrates lower threshold values (~0.55 mJ/pulse) if compared to Mo+30 system ((~0.7 mJ/pulse). In addition, the threshold values of monomers

are higher than the corresponding values for multimers. Therefore, appropriate exciton-plasmon distances in combination with stronger local fields result in a more efficient absorptive loss mitigation in hybrid plasmonic systems.

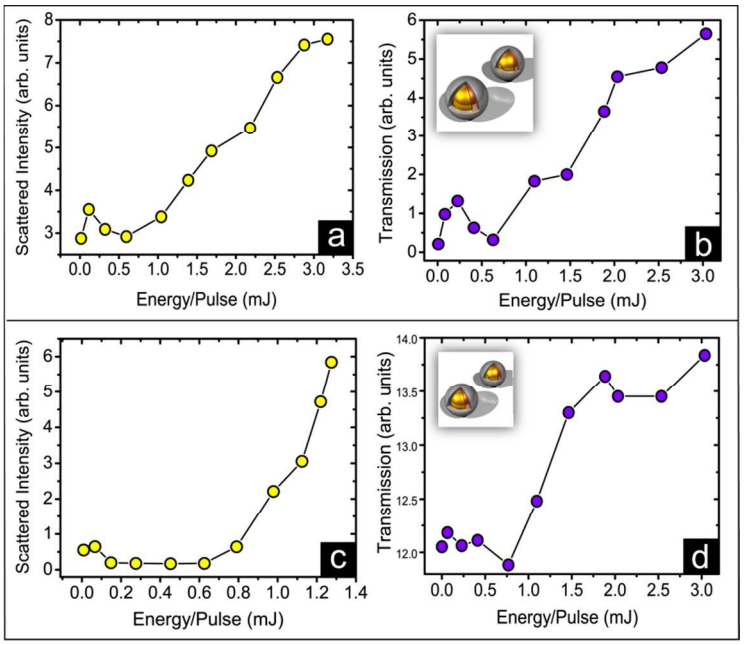

Fig. 8 Normalized Rayleigh scattering **(a,c)** and transmission **(b,d)** signals of the probe beam (532 nm) as a function of the pump energy (355 nm) for monomeric systems **(a,b)** Mo+10 and **(c,d)** Mo+30. Lower threshold values of transmittance and scattering signals are observed for Mo+10 system relative to Mo+30.

3 Conclusions

To summarize, the exciton-plasmon interplay in monomers and multimers of gain functionalized multi-shell nanostructures having different silica shell thickness (10 and 30 nm) has been investigated. Such nano-composite systems permitted a systematic investigation of the RET process between excitonic molecules and localized plasmons as a function of NP configurations and spacer thicknesses. Time-resolved fluorescence spectroscopy allowed us to investigate a remarkable resonant coupling difference between monomers and multimers. The obtained results, in combination with steady-state measurements, demonstrate that multimers experience a

more effective exciton-plasmon RET because of the enhancement of the local field related to plasmon hybridization effects. Moreover, our results show that reducing the silica shell thickness results in a better coupling strength not only between exciton and plasmon, but also between NPs in multimeric configuration, as evidenced by significant changes of fluorescence decay times. In fact, the observed enhancement of Rayleigh scattering and transmission above a critical value of gain, in correlation with inter-particle distance, have demonstrated the magnification of the local plasmon field of the gain functionalized nanostructures and the increasing of their optical transparency in presence of fluorescent molecules. The calculated plasmon field distribution and intensity of both monomeric and multimeric samples support the experimental observations.

Hence, obtained results suggest that by properly bringing gain to strongly absorptive meta-subunits can remarkably modify the imaginary part of the polarizability of these media, resulting in a reduced extinction coefficient for frequencies corresponding to the exciton-plasmon bands. In particular, engineering multimeric systems with proper values of metal-gain inter-distance can be very promising to tailor effective gain assisted plasmon hybridization processes. In the framework of bottom-up systems approach based on plasmonic materials these results may guide towards real applications of plasmonic metamaterials at optical frequencies.

3 Methods

3.1 Numerical Simulation

Simulations were conducted using COMSOL software that is full wave electromagnetic simulation software based on FEM. In simulations, the incident field is a Transverse Electromagnetic (TEM) plane wave with electric and magnetic fields in Z and Y directions respectively, while wave propagates in X direction. Along with this excitation, electric dipole

resonators are formed in Z direction. The normalized field profiles were calculated at the maximum emission wavelength of RhB dye molecules in ethanol (570 nm) and plotted in YZ cross section plane.

Gold core of nanostructures were modeled as 60 nm diameter sphere with a frequency dependent dielectric function taken from Johnson and Christy,[59] while spacer (10 nm or 30 nm) and coating shell (10 nm) were simulated using dielectric properties of silica according to Sellmeier dispersion equation.[60] The surrounding environment of nanostructures was considered as ethanol with refractive index of 1.36. The thickness of the dye shell was assumed as 5 nm, while in the simulation of the corresponding passive monomers this layer was considered as silica.

The applied dielectric function of Rhodamine B dye molecules (equation 1) in the simulation of the local fields were calculated with parameter values of $\varepsilon_h = 2.25$, $\lambda_a = 570\ nm$ ($\omega_a /2\pi = 526$ THz), $\Delta\lambda_a = 24\ nm$, and with respect to $\Delta v_a = c_0 \times \Delta\lambda_a / \lambda_a^2 = 22.2$ THz ($c_0 = 3\times10^8$ *m/s*), consequently $\Delta\omega_a = 44.2\pi$ (rad/s). Also, by considering $\tau_{21} = 3\ ns$ and $\delta_{rad} = 3\times10^8\ s^{-1}$, we have $\sigma_a = 8.25\times10^{-8}\ C^2/kg$, $\Gamma_{pump03} = 2.7\times10^9\ s^{-1}$ and $N_0 = 8.75\times10^{19}\ cm^{-3}$.

3.2 Nanoparticles Synthesis.

Gold NPs with a diameter of (60±5) nm were synthesized through the reduction of hydrogen tetrachloroaurate (III) ($HAuCl_4$) in the presence of sodium citrate ($Na_3C_6H_5O_7.2H_2O$) and sodium borohydride ($NaBH_4$) according to the procedure published by Brown *et al*.[61] Firstly, passive gold nanoparticles (without dye) were coated with a silica shell (monomer) according to the procedure published by Graf *et al*.[62] The thickness of the shell was controlled by changing the amount of silica precursor (tetraethyl orthosilicate, TEOS). The active nanoparticles (with dye)

were obtained from the passive ones by firstly grafting a Rhodamine B derivative with ethoxy-silano group, which was previously prepared by reacting Rhodamine B isothiocyanate (RhB) with aminopropyltriethoxysilane in absolute ethanol,[63] on the silica shell. To do so, an amount corresponding to 15 RhB molecules/nm^2 of silica surface was added in an ammonia (6 % v/v)/ethanol suspension of passive particles. The reactive medium was heated at 70°C during one hour. The monomers were collected by centrifugation and washed three times with absolute ethanol. A second protective silica shell of 10 nm thickness was then grown by drop wise addition of an ethanolic solution of TEOS.[64] The increase of the concentration of passive and active monomers during the addition of the TEOS solution leads to the formation of multimers which are the mixture of dimers, trimers, quadrimers, heptamers, etc. These mulitmers are formed as a result of collisions between monomer particles and are permanently fixed via the hydrolysis and condensation of TEOS molecules on their surface.[65] Synthesized multimers were filtered via ultrafiltration membranes to separate monomers from multimers. However, filtrating of all monomers is not experimentally achievable. Statistical analyses on several multimeric nanostructures have been performed in order to determine the core average size and the shell average thickness. The average core diameter is about 63.8 nm. For Mu+10 and Mo+10 samples (with 10 nm exciton-plasmon silica gap and 10 nm protective layer) the average shell thickness is approximately 18 nm, while for Mu+30 and Mo+30 samples (with 30 nm exciton-plasmon silica gap and 10 nm protective layer) is about 44 nm.

3.3 Characterization and Measurements.

Extinction bands were measured by means of a spectrophotometer (Cary5E by Varian), whereas the Steady-state emission spectra were recorded on a HORIBA Jobin-Yvon Fluorolog-3 FL3-211

spectrometer equipped with a 450 W xenon arc lamp, double grating excitation and single-grating emission monochromators (2.1 nm/mm dispersion; 1200 grooves/mm), and a Hamamatsu R928 photomultiplier tube. Emission and excitation spectra were corrected for source intensity (lamp and grating) and emission spectral response (detector and grating) by standard correction curves. TEM observations were performed with a Hitachi H-600 microscope operating at 75 kV, where particles were cast on a glass substrate by leaving a drop of a diluted suspension evaporating.

The fluorescence lifetime of the two systems was acquired with respect to that of pure dye solution, by means of advanced fluorescence lifetime spectrometer (Edinburgh, FLS980 Series) using TCSPC data option. The used system, an ultrafast time-resolved fluorescence spectroscopic instrument, consists of a Ti: Sapphire pulsed laser as a tunable excitation source in the 680-1080 nm range (repetition rate = 80 MHz, pulse width = 140 fs, by Coherent Inc.), represents the core of a customized set-up that presents a Pulse Picker used to decrease the repetition rate in the range between 1 to 5 MHz, in order to be synchronized with a multi pronged spectrofluorometer able to perform both steady state measurements and TCSPC investigations. The excitation laser source has been adjusted at 750 nm, in order to perform time-resolved measurements on samples. A Second Harmonic Generation (SHG) module is used to decrease the excitation wavelength in the range of 340-540 nm (blue beam). All the above mentioned investigations are performed inside the spectrofluorometer chamber (sample position S1). A multi channel plate, synchronized with incoming pulses is used to acquire the fluorescence decay lifetime in the proper temporal range. Broadband half-wave plate (λ/2) and high damage threshold polarizer (P) are used to control the power of excitation pulses. The mounted periscope (PE) has been used to have an in-plane beam at different height. The photons

collected at the detector are correlated by a time-to-amplitude converter (TAC) to the excitation pulse. Signals were collected by using a photon counting module, and data analysis was performed using the commercially available F900 software. The fit of data has been acquired by instrument software and quality of fit was assessed by minimizing the reduced χ^2 function and visual inspection of the weighted residuals.

Furthermore, Förster non-radiative energy transfer processes necessary to mitigate the high metal losses can be observed through indirect experiments. All of them are based on a pump-probe setup. The sample is optically pumped with 4 ns pulses of the third harmonic of a Nd:YAG laser (Brio by Quantel), λ = 355 nm. A probe beam (CW diode-pumped solid-state laser at 532 nm by Laser Quantum), with a fixed low power, was focused within the excitation region of the sample. The probe wavelength was chosen in the proximity of the overlapping region between dye fluorescence and plasmon band maxima, where localized surface plasmon modes are expected. The probe light emitted, scattered, or transmitted by Au NPs (λ @ 532 nm) was collected by an optical fiber together with the emission of dye, in a position depending on the particular experiment. The fiber was positioned at the angle of 70° relative to the beam propagation direction for scattering (90° for fluorescence) experiment, within several millimeters from the cuvette; transmission signals were acquired far from the sample, on the same pump beam direction and with a high neutral filter in front of the fiber head, in order to prevent any possible signal different from the probe one (high stable power).

Acknowledgment

The authors thank C. Versace, M. Albani, A. Vallecchi, N. Scaramuzza and M. La Deda for the fruitful scientific discussions. We acknowledge support of the Ohio Third Frontier Project,

"Research Cluster on Surfaces in Advanced Materials (RC-SAM) at Case Western Reserve University". The research leading to these results has received funding from the EU-FP7 (FP7/2008) METACHEM Project under Grant Agreement No. 228762.

References

1 G. Raschke, S. Kowarik, T. Franzl, C. Sönnichsen, T. A. Klar, J. Feldmann, A. Nichtl, K. Kürzinger, *Nano Lett*., 2003, **3**, 935.

2 I. H. El-Sayed, X. Huang, M. A. El-Sayed, *Nano Lett*., 2005, **5**, 829.

3 A. F. Scarpettinia, N. Pellegrib, A. V. Bragasa, *Opt. Commun.,* 2009, **282**, 1032.

4 V. Zharov, V. Galitovsky, M. Viegas, *Appl. Phys. Lett*., 2003, **83**, 4897.

5 K. R. Catchpole, A. Polman, *Opt. Express,* 2008, **16**, 21793.

6 K. Kneipp, Y. Wang, H. Kneipp, L. T. Perelman, I. Itzkan, R. Dasari, M. S. Feld, *Phys. Rev. Lett.,* 1997, **78**, 1667.

7 A. M. Michaels, M. Nirmal, L. E. Brus*, J. Am. Chem. Soc.,* 1999, **121**, 9932.

8 P. M. Tessier, O. D. Velev, A. T. Kalambur, J. F Rabolt, A. M. Lenhoff, E. W. Kaler, *J. Am. Chem. Soc.,* 2000, **122**, 9554.

9 R. A. Reynolds, C. A. Mirkin, R. L. Letsinger, *J. Am. Chem. Soc.,* 2000, **122**, 3795.

10 J. B Pendry, *Phys. Rev. Lett.,* 2000, **85**, 3966.

11 W. Cai, U. K. Chettiar, A. V. Kildishev, V. M. Shalaev*, Nat. Photonics,* 2007, **1**, 224.

12 M. A. Vincenti, S. Campione, D. de Ceglia, F. Capolino, M. Scalora, *New J. Phys.,* 2012, **14**, 103016.

13 A. Fang, T. Koschny, M. Wegener, C. M. Soukoulis, *Phys. Rev. B,* 2009, **79**, 241104.

14 S. Campione, F. Capolino, *Nanotechnology,* 2012, **23**, 235703.

15 S. Campione, S. Steshenko, M. Albani, F. Capolino, *Opt. Express,* 2011, **19**, 26027.

16 M. A. Noginov, V. A. Podolskiy, G. Zhu, M. Mayy, M. Bahoura, J. A. Adegoke, B. A Ritzo, K. Reynolds, *Opt. Express* 2008, **16**, 1385.

17 C. Garcia, V. Coello, Z. Han, I. P. Radko, S. I. Bozhevolnyi, *Opt. Express,* 2012, **20**, 7771.

18 B. Peng, Q. Zhang, X. Liu, Y. Ji, H. V. Demir, C. H. A. Huan, T. C. Sum, Q. Xiong, *ACS Nano,* 2012, **6**, 6250.

19 A. De Luca, R. Dhama, A. R. Rashed, C. Coutant, S. Ravaine, P. Barois, M. Infusino, G. Strangi *Appl. Phys. Lett.,* 2014, **104**, 103103.

20 F. Cannone, G. Chirico, A. R. Bizzarri, S. Cannistraro, *J. Phys. Chem. B*, 2006, **110**, 16491.

21 C. Xue, Y. Xue, L. Dai, A. Urbas, Q. Li, *Adv. Optical Mater.*, 2013, **1**, 581.

22 M. P. Singh, G. F. Strouse, *J. Am. Chem. Soc.*, 2010, **132**, 9383.

23 S. Halivni, A. Sitt, I. Hadar, U. Banin, *ACS Nano*, 2012, **6**, 2758.

24 T. Soller, M. Ringler, M. Wunderlich, T. A. Klar, J. Feldmann, *Nano Lett.*, 2007, **7**, 1941.

25 P. Viste, J. Plain, R. Jaffiol, A. Vial, P. M. Adam, P. Royer, *ACS Nano, 2010*, **4**, 759.

26 T. Ozel, P. L. Hernandez-Martinez, E. Mutlugun, O. Akin, S. Nizamoglu, I. Ozge Ozel, Q. Zhang, Q, Qihua Xiong, H. Volkan Demir, *ACS Nano*, 2013, **13**, 3065.

27 A. De Luca, M. P. Grzelczak, I. Pastoriza-Santos, L. M. Liz-Marzán, M. La Deda, M. Striccoli, G. Strangi, *ACS Nano*, 2011, **5**, 5823.

28 G. Strangi, A. De Luca, S. Ravaine, M. Ferrie, R. Bartolino, *Appl. Phys. Lett.,* 2011, **98**, 251912.

29 A. De Luca, M. Ferrie S. Ravaine, M. La Deda, M. Infusino, A. R. Rashed, A. Veltri, A. Aradian, N. Scaramuzzaa, G. Strangi, *J. Mater. Chem.,* 2012, **22**, 8846.

30 D. W. Brandl, N. A. Mirin, P. Nordlander, *J. Phys. Chem. B,* 2006, **110**, 12302.

31 H. Wang, D. W. Brandl, P. Nordlander, N. J. Halas, *Acc. Chem. Res.,* 2007, **40**, 53.

32 P. Nordlander, C. Oubre, E. Prodan, K. Li, and M.I. Stockman, *Nano Lett*., 2004, **4**, 899.

33 S. C. Yang, H. Kobori, C. L. He, M. H. Lin, HY. Chen, C. Li, M. Kanehara, T. Teranishi, S. Gwo, *Nano Lett*., 2010, **10**, 632.

34 S. J. Barrow, X. Wei, J. S. Baldauf, A. M. Funston, P. Mulvaney, *Nat. Commun*., 2012, **3**, 1275.

35 C. S. Yun, A. Javier, T. Jennings, M. Fisher, S. Hira, S. Peterson, B. Hopkins, N. O. Reich, G. F. Strouse, *J. Am. Chem. Soc.,* 2005, **127**, 3115.

36 T. Pons, I. L. Medintz, K. E. Sapsford, S. Higashiya, A. F. Grimes, D. S English, H. Mattoussi, *Nano Lett.,* 2007, **7**, 3157.

37 J. Griffin, A. K. Singh, D. Senapati, P. Rhodes, K. Mitchell, B. Robinson, E. Yu, P. C. Ray, *Chem. Eur. J.,* 2009, **15**, 342.

38 T. Förster, *Ann. Phys. Berlin,* 1948, **437**, 55.

39 L. M. Liz-Marzan, M. Giersig, P. Mulvaney, *Langmuir,* 1996, **12**, 4329.

40 A. E. Schlather, N. Large, A. S. Urban, P. Nordlander, N. J. Halas, *Nano lett.,* 2013, **13**, 3281.

41 J. Rodrıguez-Fernandez, I. Pastoriza-Santos, J. Perez-Juste, F. J. Garcıa de Abajo, L. M. Liz-Marzan, *J. Phys. Chem. C,* 2007, **111**, 13361.

42 P. W. Milonni, J. H. Eberly, Laser Physics, Wiley: New York, 2010.

43 A. Fang, T. Koschny, M. Wegener, C. M. Soukoulis, *Phys. Rev. B,* 2009, **79**, 241104.

44 S. Campione, M. Albani, F. Capolino, *Opt. Mater. Express,* 2011, **1**, 1077.

45 Gersten, J. I.; Nitzan, *A. Surf. Sci.,* 1985, **158**, 165.

46 E. Prodan, C. Radloff, N. J. Halas, P. Nordlander, *Science,* 2003, **302**, 419.

47 A. P. Demchenko, Advanced Fluorescence Reporters in Chemistry and Biology, Springer: Berlin, 2011.

48 S. Özçelik, D. L. Akins, *J. Phys. Chem. B,* 1999, **103**, 8926.

49 J. R. Lakowicz, *Anal. Biochem*., 2001, **298**, 1.

50 J. R. Lakowicz, Principles of Fluorescence Spectroscopy, Springer: New York, 2006.

51 Y. Li, Q. Li, Z. Zhang, H. Liu, X. Lu, Y. Fang, *Plasmonics*, 2015, **10**, 271.

52V. Pustovit, F. Capolino, A. Aradian, *J. Opt. Soc. Am. B,* 2015, **32**, 188.

53 V. N. Pustovit, T. V. Shahbazyan, 2009, *Phys. Rev. Lett.,* **102**, 077401.

54 J. R. Lakowicz, *Anal Biochem.,* 2005, **337**, 171.

55 M. Ferriè, N. Pinna, S. Ravaine, R. A. L. Vallèe, *Opt. Express,* 2011, **19**, 17697.

56 N. M. Lawandy, *Appl. Phys. Lett.,* 2004, **85**, 5040.

57 S. Bhowmick, S. Saini, V. B. Shenoy, B. Bagchi*, J. Chem. Phys.,* 2006, **125**, 181102.

58 J. Seelig, K. Leslie, A. Renn, S. K1uhn, V. Jacobsen, M. van de Corput, C. Wyman, and V. Sandoghdar, *Nano Lett.,* 2007, **7**, 685.

59 P. B. Johnson, R. W. Christy*, Phys. Rev. B,* 1972, **6**, 4370.

60 I. H. Malitson, *J. Opt. Soc. Am.,* 1965, **55**, 1205.

61 K. R. Brown, D. G. Walter, M. J. Natan, *Chem. of Mater.,* 2000, **12**, 306.

62 C. Graf, A. van Blaaderen, *Langmuir,* 2002, **18**, 524.

63 X. Gao, J. He, L. Deng, H. Cao, *Opt. Mater.,* 2009, **31**, 1715.

64 S. Kang, S. I. Hong, C. R. Choe, M. Park, S. Rim, J. Kim, *Polymer,* 2001, **42**, 879.

65 M. Ibisate, Z. Zou, Y. Xia, *Adv. Funct. Mater*., 2006, **16**, 1627.